J. Fluid Mech. (1990), *vol.* 215, *pp.* 209–227
Printed in Great Britain

Transition to oscillatory motion in rotating channel flow

By W. H. FINLAY
Department of Mechanical Engineering, University of Alberta, Edmonton, Alberta, Canada T6G 2G8

(Received 24 March 1989 and in revised form 8 November 1989)

A numerical study of the transition from steady to oscillatory streamwise-oriented vortices in fully developed rotating channel flow is presented. The principal results are obtained from three-dimensional, spectral simulations of the incompressible time-dependent Navier–Stokes equations. With increasing Reynolds number, two transitions that cause the steady, periodic array of two-dimensional vortices (roll cells) to develop waves travelling in the streamwise direction are discovered. The linear stability of two-dimensional vortices to wavy perturbations is examined. Associated with the two transitions are two different wavy vortex flows: WVF1 and WVF2. WVF2 is very similar to undulating vortex flow found in curved channel flow simulations (Finlay, Keller & Ferziger 1988) and to wavy Taylor vortex flow. WVF2 is only possible at low rotation rates. In contrast, the dissimilar WVF1 occurs for all rotation rates examined, has shorter streamwise wavelength and, for sufficiently high Reynolds number, has much higher linear growth rate than WVF2. For low rotation rates, WVF1 is similar to curved channel flow twisting vortices, but at higher rotation rates appears dissimilar. Several key qualitative features are discussed that suffice in describing all these wavy vortex flows.

1. Introduction

At sufficiently small Reynolds number, Re, the velocity in infinite-span rotating channel flow is purely streamwise. At higher Re, secondary flow containing two-dimensional, streamwise-oriented vortices (roll cells) can develop, owing to an imbalance of Coriolis and pressure forces. At still higher Re, these vortices can develop waves travelling in the streamwise direction. In this work, the linear stability of periodic two-dimensional vortices to travelling waves is examined. Three-dimensional, nonlinear wavy vortices resulting from this instability are examined using numerical simulations of the Navier–Stokes equations. A better understanding of the transitions leading to turbulence in rotating channel flow may yield a better understanding of the physics of transition in general and in other geometries such as coolant flow in turbine blades, flow inside impellers of centrifugal pumps, and geophysical flows such as in deep sea basins partitioned by submarine ridges.

The flow geometry is shown in figure 1. The channel spacing is d. Throughout this work, velocities will be non-dimensionalized by the bulk velocity (i.e. the average mean streamwise velocity) $\bar{U}$ and lengths will be non-dimesionalized by d. The Reynolds number is $Re = \bar{U}d/\nu$. The coordinate system is aligned such that (x, y, z) are streamwise, normal, and spanwise directions respectively, with the channel centreline defined as $y = 0$. The rotation number is $Ro = \Omega d/\bar{U}$, where Ω is the dimensional angular speed of rotation about the z-axis. A non-dimensional spanwise

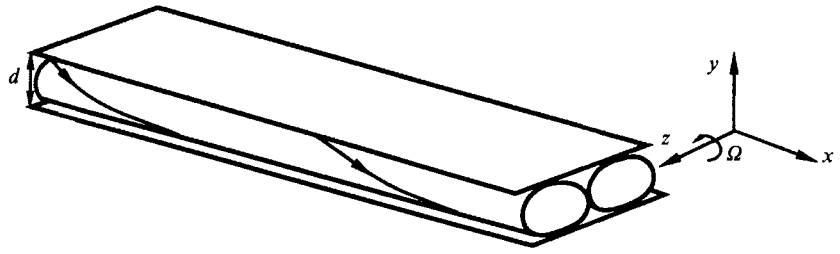

FIGURE 1. Schematic drawing of rotating channel flow. The flow is periodic in z.

Ro	Re_c	α_c
0.084	146.6941	4.16
0.1	136.3972	4.19
0.5	88.5994	4.91
1.5	183.0970	8.13

TABLE 1. The critical Reynolds number, Re_c, and wavenumber, α_c, for instability of rotating plane Poiseuille flow to two-dimensional vortices are given for the rotation rates, Ro, used herein.

wavenumber is $\alpha = 2\pi d/\lambda$, where λ is the spanwise vortex spacing. Rotating channel flow experiments have finite aspect ratio $\Gamma = h/d$, where h is the spanwise dimension of the channel.

For infinite-span channels and low Re, the streamwise velocity profile is the same as plane Poiseuille flow, but there is a normal pressure gradient when $Ro \neq 0$. This flow will be called rotating plane Poiseuille flow, and is inviscidly unstable to two-dimensional vortices when $0 < Ro < 3$ (cf. Tritton & Davies 1985). For given α and Ro, linear neutral stability analysis predicts the neutrally stable Reynolds number Re_{ns} above which two-dimensional vortices have positive linear growth rates. For given Ro, the minimum of the neutral stability curve $Re_{ns}(\alpha)$ occurs at the critical Reynolds number Re_c and the critical wavenumber α_c. One-dimensional flow occurs for $Re < Re_c$; two-dimensional vortices can occur for $Re > Re_c$. Previous authors (cf. Tritton & Davies 1985 for a literature review, and also Alfredsson & Persson 1989) have found Re_{ns}, Re_c, and α_c for various Ro; Re_c is finite only in the range $0 < Ro < 3$, with the minimum occurring at $Re_c = 88.6$, $Ro = 0.5$. Table 1 gives Re_c and α_c for the Ro considered here. Also assuming spanwise periodicity, Finlay (1989) examines a perturbation expansion for two-dimensional vortices in curved or rotating channels and truncates this expansion to provide a Stuart–Watson weakly nonlinear analysis of two-dimensional vortices that is accurate near the neutral stability curve (see also Ng *et al.* 1989). The Re-dependence implied by the full perturbation expansion is compared with two-dimensional, fully nonlinear vortices obtained by the same numerical method used here.

Above $Re = 7696$, rotating plane Poiseuille flow becomes linearly unstable to Tollmien–Schlichting waves, but in this work Re is well below this value or even that needed for subcritical transitions of plane Poiseuille flow.

For large but finite aspect ratio, rotating plane Poiseuille flow is modified by single end vortices located near $z = \pm\frac{1}{2}\Gamma$. Roll cells occur in the interior for Re, Ro nearly within the range predicted by infinite-span linear stability analysis (Hart

1971; Lezius & Johnston 1976; Speziale & Thangam 1983; Alfredsson & Persson 1989). Alredsson & Persson (1989) provide experimental roll-cell spacings in a channel with $\Gamma = 60$. Flows with end vortices, $\Gamma = 8$, and with or without interior vortices have been studied numerically by Speziale & Thangam (1983); Thangam & Speziale (1985) consider heating of the $y = +\frac{1}{2}$ wall. Speziale (1982) examines numerical solutions for $\Gamma = 2$, and finds the two-cell flow can change to a four-cell flow for moderate Ro and high Re. Kuz'minskii, Smirnov & Yurkin (1983), and Smirnov & Yurkin (1983) provide experimental results on the number of cells occurring in rectangular channels with $\Gamma < 7.2$. Khesgi & Scriven (1985) examine a two–four cell bifurcation for $\Gamma = 1$ using continuation methods, finding hysteresis. They also examine geostrophic flow without vortices, which occurs for $Ro \gg 1$, $Re \ll Ro$. Thangam & Speziale (1987) study non-Newtonian secondary flows for a square rotating duct. All theoretical papers cited in this paragraph assume that the flow is independent of streamwise coordinate, i.e. the flow is two-dimensional.

Smirnov & Yurkin (1983), Smirnov *et al.* (1983) mention regular oscillations of vortices in square and rectangular channels, which cause the flow to depend on streamwise position. For $\Gamma = 60$, Alfredsson & Persson (1989) provide flow visualizations which indicate periodic waves travelling on the roll cells. They suggest these are wavy vortices like those occurring in curved channel flow (Finlay, Keller & Ferziger 1988). Wavy vortices have also been observed by Yang & Kim (1990). Wavy vortex flows have been studied in Taylor–Couette flow (cf. DiPrima & Swinney 1985), Rayleigh–Bénard convection (where they are called oscillatory convection rolls, cf. Busse 1985), and curved channel flow (Finlay *et al.* 1988). Experimental observations suggest that such flows may occur in rotating channel flow also. In this work, the transition from two-dimensional vortices to wavy rotating channel vortices is examined in §3. Details of nonlinear wavy vortices are given in §4. Rotation and Reynolds numbers in the range $0.084 \leqslant Ro \leqslant 1.5$ and $Re < 600$ are considered. The numerical method used to obtain these results is briefly described in §2. Spanwise and streamwise periodicity is imposed, preventing examination of finite-span features. In addition, the flow is assumed fully developed; that is, streamwise development or entrance length effects are not considered here.

2. Code implementation

Using the numerical method of Moser, Moin & Leonard (1983), we obtain three-dimensional time-dependent solutions of the incompressible Navier–Stokes equations for a rotating channel. Periodic boundary conditions are used in the spanwise and streamwise directions. A pseudo-spectral method based on expansion functions that satisfy the continuity equation and the boundary conditions is used. Time-advancement is implicit (Crank–Nicholson) for viscous terms and explicit (second-order Adams–Bashforth) for nonlinear and Coriolis terms. Effects of centrifugal force are absorbed in the hydrostatic pressure. The code is a modification of the one used to study wavy Taylor vortices by Moser *et al.* (1983), wavy Dean vortices by Finlay *et al.* (1988), weakly nonlinear two-dimensional curved or rotating channel vortices by Finlay (1989), and to perform a direct simulation of turbulence in the curved channel (Moser & Moin 1984, 1987).

The solution progresses in time with constant mass flux imposed. To eliminate aliasing errors, the nonlinear terms are evaluated in real space on a grid with $\frac{3}{2}$ as many grid points in each direction as the number of modes used in transform space (cf. Canuto *et al.* 1988).

3. Linear stability of two-dimensional vortices to wavy perturbations

We examine the linear stability of two-dimensional vortices to wavy disturbances by writing the velocity as

$$v(x,y,z,t) = u(y,t)\,e^{(\sigma-i\omega)t}\,e^{i\beta x} + v^{2D}(y,z), \tag{3.1}$$

where $v^{2D}(y,z)$ represents a fully developed, two-dimensional vortex flow obtained using the code. The physical velocity field is the real part of (3.1). The complex temporal growth rate, $\sigma - i\omega$, allows oscillatory growth or decay. The parameter β is a given real-valued streamwise wavenumber. Disturbances with spanwise period different to that of v^{2D} are not considered. Equation (3.1) implies that the wavy disturbance travels in the streamwise direction with speed

$$c = \omega/\beta. \tag{3.2}$$

At given α and Ro, there is an Re above which v^{2D} with only one pair of vortices per period cannot be obtained because of vortex doubling (Khesgi & Scriven 1985 examine a similar result for a square channel). Similar behaviour occurs for Dean vortices (Finlay *et al.* 1988) and Taylor vortices (e.g. Meyer-Spasche & Keller 1985). The Re-range examined in this section extends near to this vortex doubling limit. Ligrani & Niver (1988) observe spanwise splitting (with subsequent merging) of vortices in curved channel flow. Figure 6 of Alfredsson & Persson (1989) probably indicates that vortex splitting occurs in rotating channel flow as well. Such results may be associated with the stability of two-dimensional vortices to disturbances with different spanwise wavenumber (for example, Eckhaus instability), and are not examined here.

For given (Re, α, Ro, β) we examine the stability of wavy perturbations by substituting (3.1) into the Navier–Stokes equations. We could linearize the resulting partial differential equations and study the eigenvalue problem, but instead choose to use the three-dimensional nonlinear code. We choose the streamwise length of the computational region to be $2\pi/\beta$. The initial conditions have $e^{i\beta x}$ streamwise variation, are divergence free, and are a low-amplitude ($< 0.01\,\%\,\bar{U}$) wavy perturbation from v^{2D} (given in Finlay *et al.* 1987). The solution progresses in time until $e^{(\sigma-i\omega)t}$ time dependence is found. The first streamwise Fourier mode of this solution is the desired eigensolution. We use 19 spanwise Fourier modes, 7 streamwise Fourier modes, and Chebyshev polynomials up to order 32 in the normal direction. Observations of spatial energy spectra showed this resolution is sufficient.

Two-dimensional vortices have reflection symmetry about their upflow and downflow planes, i.e. the (x,y)-planes where $v_z = 0$ (Finlay 1989). A wavy perturbation is called 'in phase' if it satisfies the same reflection symmetry property. an out-of-phase mode has reflection symmetry about planes shifted by $\frac{1}{4}\lambda$ from the downflow and upflow planes. In general, a wavy perturbation is neither in phase nor out of phase, but is a linear combination of these two types of modes. Dean vortices, Taylor vortices (for radius ratio $\eta > 0.5$ and a stationary outer cylinder), and Rayleigh–Bénard convection rolls (for moderate Prandtl number) are linearly stable to in-phase wavy disturbances (Finlay *et al.* 1988; Davey, DiPrima & Stuart 1968; Jones 1981, 1985; Bolton, Busse & Clever 1986). Thus, instability is determined by disturbances which are out of phase. For the Re, α, β, Ro considered, all small-amplitude growing disturbances of the form (3.1) are out of phase in rotating channel flow as well. Fully developed, nonlinear, three-dimensional rotating channel vortices are neither in phase nor out of phase.

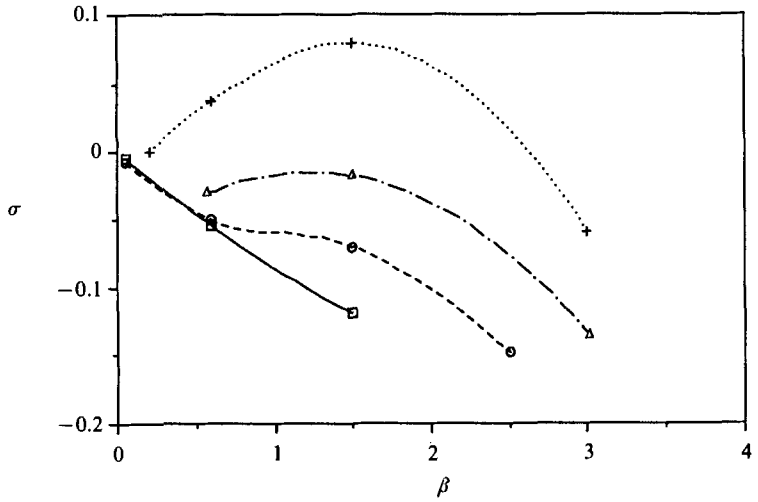

FIGURE 2. Linear growth rates, σ, of wavy disturbances to two-dimensional vortices are shown as a function of streamwise wavenumber, β, at $Ro = 1.5$, $\alpha = 10$ and Re as follows: □, ——, $Re = 1.529Re_c$; ○, — — — —, $Re = 2.021Re_c$; △, —·—, $Re = 2.512Re_c$; +, ·····, $Re = 3.277Re_c$. Lines are included only to guide the eye.

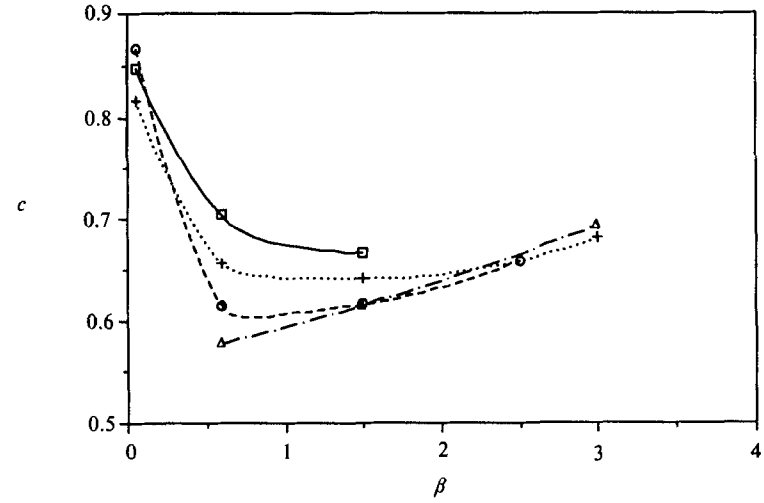

FIGURE 3. Wave speeds, c, of small-amplitude wavy disturbances to two-dimensional vortices are shown as a function of streamwise wavenumber, β, at $Ro = 1.5$, $\alpha = 10$ and Re as follows: □, ——, $Re = 1.529Re_c$; ○, — — — —, $Re = 2.021Re_c$; △, —·—, $Re = 2.512Re_c$; +, ·····, $Re = 3.277Re_c$.

Figure 2 gives $\sigma(\beta)$ for several Re at $Ro = 1.5, \alpha = 10$. By interpolation, two-dimensional vortices are first unstable (with increasing Re) to wavy disturbances at $Re \equiv Re'_{ns} \approx 2.7Re_c$ and $\beta \approx 1.5$. At $\alpha = 8$, $\sigma(\beta)$ behaves similarly except that $Re'_{ns} \approx 2Re_c$ is lower. In contrast, for wavy Taylor vortices with $\eta > 0.75$ (Jones 1981, 1985), curved channel undulating vortices (Finlay *et al.* 1988), and oscillatory Rayleigh–Bénard convection rolls with stress free boundaries (Busse 1972), instability occurs first at the smallest β geometrically possible ($\beta = 1/r_c$ for the curved geometries where r_c is the centreline radius of curvature, and $\beta = 0$ for convection).

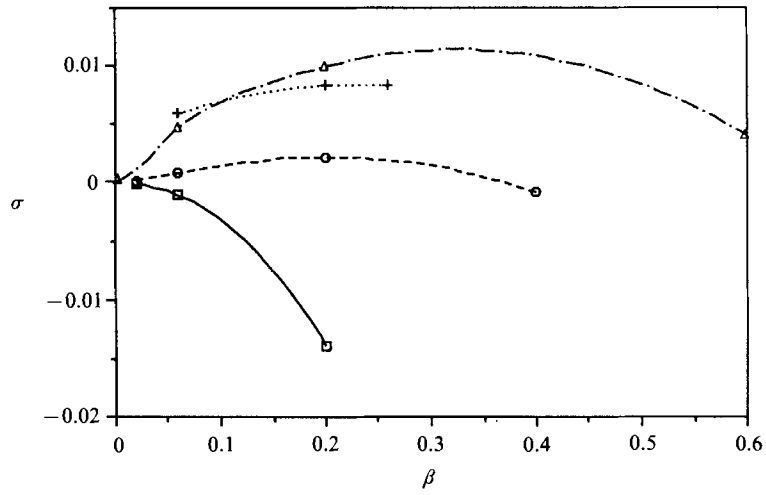

FIGURE 4. Linear growth rate, σ, of wavy disturbances are shown as a function of $\beta \leqslant 0.6$ for $Ro = 0.5$, $\alpha = 8$, and Re as follows: □, ——, $Re = 1.354Re_c$; ○, — — — —, $Re = 1.693Re_c$; △, —·—, $Re = 2.032Re_c$; +, ·····, $Re = 2.596Re_c$.

Oscillatory instability of Rayleigh–Benard convection rolls with the more realistic rigid boundaries (Clever & Busse 1974), and the transition to twisting vortices in curved channel flow (Finlay *et al.* 1988) first occur at β considerably higher than the smallest.

Figure 3 gives $c(\beta)$ at the same Ro, α, Re as figure 2; $\omega = c\beta$ is approximately linear in β. The wave speed, c, varies non-monotonically with Re. At $\alpha = 8$, $c(\beta)$ is qualitatively similar.

When Ro is lowered to $Ro = 0.5$, and $\alpha = 6$, $\sigma(\beta)$ is similar to that at $Ro = 1.5$, except $Re'_{ns} \approx 3.0Re_c$. We choose $\alpha = 6$ because it is near that observed experimentally by Alfredsson & Persson (1989) for this Ro.

For the α, Re, Ro considered so far in this section, σ approaches zero as $\beta \to 0$, and Re'_{ns} is determined by $\beta \approx 1.5$. For small β, positive values of σ occur only when Re is considerably greater than Re'_{ns}. In contrast, at $Ro = 0.5$ and $\alpha = 8$, wavy disturbances with $\beta \to 0$ are the first to become unstable with increasing Re. Figure 4 gives $\sigma(\beta)$ for several Re at $\alpha = 8$, $Ro = 0.5$. Although $\beta \to 0$ is first unstable, modes with $\beta > 0$ have larger positive growth rates for higher Re. Figure 5 shows $\sigma(\beta)$ for a larger range of β. The disturbance with largest positive growth rate shifts to much higher β when Re increases above a certain value. For some Re, there are two local maxima in $\sigma(\beta)$. To the author's knowledge, this behaviour is not observed for oscillatory Rayleigh–Benard convection or Taylor–Couette flow with only the inner cylinder rotating, but does occur in curved channel flow (Finlay *et al.* 1988). It should be noted that the method we use to obtain σ yields only the largest eigenvalue. In fact, preliminary data obtained by solving the eigenvalue problem directly with a spectral tau method show that the two local maxima correspond to two different eigenmodes, each having a $\sigma(\beta)$-curve similar to an inverted parabola. When only the maximum σ between the two modes is plotted, two maxima can occur. The two maxima are well separated and we define β_1 and β_2 as the positions of the maxima with higher and lower β, respectively; both depend on Re, α, Ro. As shown in the following section, the wavy vortex flows corresponding to the two ranges of β are dissimilar. We use the abbreviations WVF1 and WVF2 to describe wavy vortices

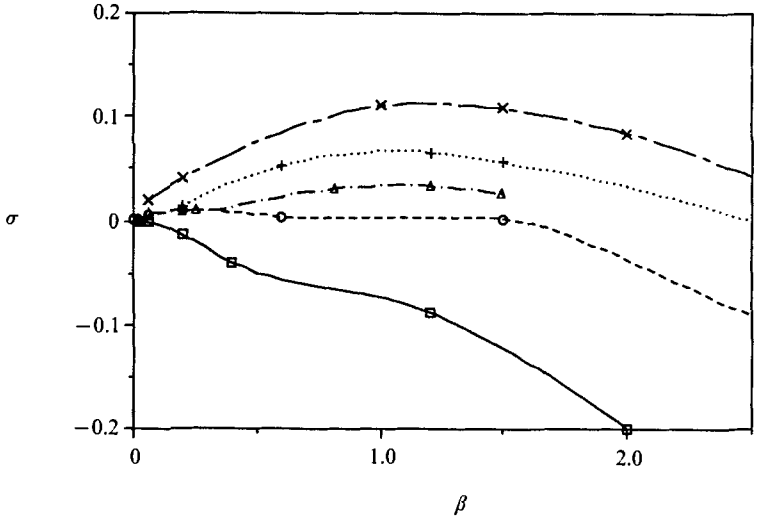

FIGURE 5. Linear growth rate, σ, of wavy disturbances are shown as a function of β for $Ro = 0.5$, $\alpha = 8$, and Re as follows: □, ——, $Re = 1.354Re_c$; ○, — — — —, $Re = 2.032Re_c$; △, —·—, $Re = 2.596Re_c$; +, ·····, $Re = 3.160Re_c$; ×, — — —, $Re = 4.515Re_c$.

with β near β_1 and β_2, respectively. With increasing Re, two-dimensional vortices first become unstable to WVF2 always for $\beta \to 0$, whereas instability to WVF1 occurs first for β not near zero; this differences distinguishes the two modes. For $Ro = 0.5$, $\alpha = 8$, and increasing Re, WVF2 occurs first for $\beta \to 0$ at $Re \equiv Re''_{ns} \approx 1.5Re_c$; WVF1 first occurs for $Re'_{ns} \approx 2.0Re_c$ and $\beta \approx 1.0$. Finlay *et al.* (1988) used the terms 'twisting' and 'undulating' Dean vortices to mean β_1 and β_2, respectively, in curved channel flow at $\eta = 0.975$. Here, 'undulating' vortex flow will be used to mean WVF2, because of the similarity to undulating Dean vortices flow (see §4). WVF1 is similar to twisting Dean vortex flow for some Ro but different at others, so 'twisting vortices' will not be used here to mean WVF1. For the Re shown in figure 5, $\sigma(\beta_1)$ increases monotonically with increasing Re. In contrast, $\sigma(\beta_2)$ increases from zero at Re''_{ns} to a maximum at some Re and then decreases with further increases in Re. We define Re_β as the Reynolds number at which $\sigma(\beta_1) = \sigma(\beta_2)$. By interpolation, $Re_\beta \approx 2.2Re_c$ for $\alpha = 8$, $Ro = 0.5$; Re'_{ns}, Re_β and Re''_{ns} are functions of Ro and α. For example, at $Ro = 1.5$, Re'_{ns} increases between $\alpha = 8$ and 10, but at $Ro = 0.5$, Re'_{ns} decreases between $\alpha = 6$ and 8. If both modes become unstable with increasing Re, then, for the parameter range explored, $Re''_{ns} < Re'_{ns}$, i.e. WVF2 occurs first with increasing Re. For Re sufficiently greater than Re_β, $\sigma(\beta_1) \gg \sigma(\beta_2)$.

The behaviour of the non-dimensional wave speed, c, as a function of β and Re for $\alpha = 8$, $Ro = 0.5$ is given in figure 6. An abrupt change in $c(\beta)$ occurs between the two modes. The wave speed is asymptotic to a constant for large β in the range considered, which is also true for twisting vortices in curved channel flow (Finlay *et al.* 1988). At $Ro = 0.5$, c is a relatively weak function of Re, as in curved channel flow (Finlay *et al.* 1988) and Taylor–Couette flow (King *et al.* 1984). Wave speeds for WVF1 with $\alpha = 6$, $Re = 3.160Re_c$, $Ro = 0.5$ are included in figure 6 to show the small variation with α, especially for $\beta > 0.5$. For undulating vortices, $\omega(\beta)$ is linear for small β, and $\omega \to 0$ as $\beta \to 0$, as in Rayleigh–Bénard convection with stress free boundaries (Busse 1972).

At $Ro = 0.5$, only WVF1 has positive linear growth rates when $\alpha = 6$, but both

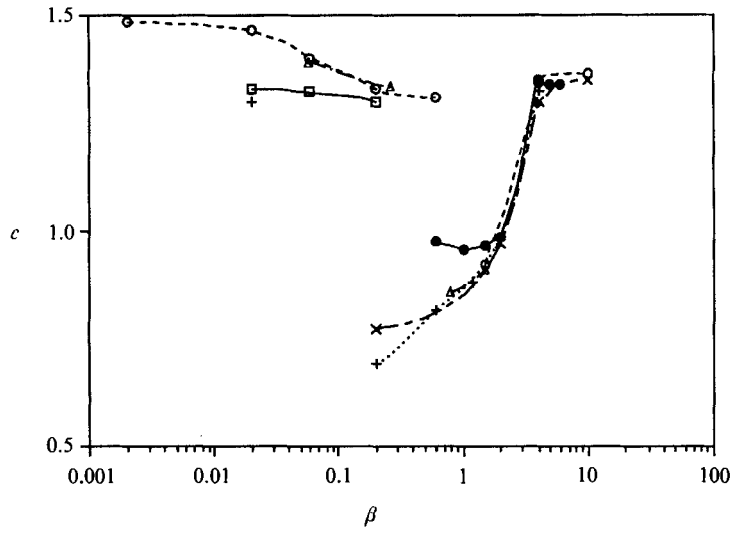

FIGURE 6. Wave speeds, c, of small-amplitude wavy disturbances to two-dimensional vortices are shown as a function of streamwise wavenumber, β, at $Ro = 0.5$, $\alpha = 8$ and Re as follows: □, ——, $Re = 1.693Re_c$; ○, — — — —, $Re = 2.032Re_c$; △, —·—, $Re = 2.596Re_c$; +, ·····, $Re = 3.160Re_c$; ×, — — —, $Re = 4.515Re_c$. Data for $\alpha = 6$, $Re = 3.160Re_c$, $Ro = 0.5$ is shown as ●, ——. Data for WVF1 is to the lower right, and is not joined by lines to the data for WVF2 at the upper left, even though Re may be the same.

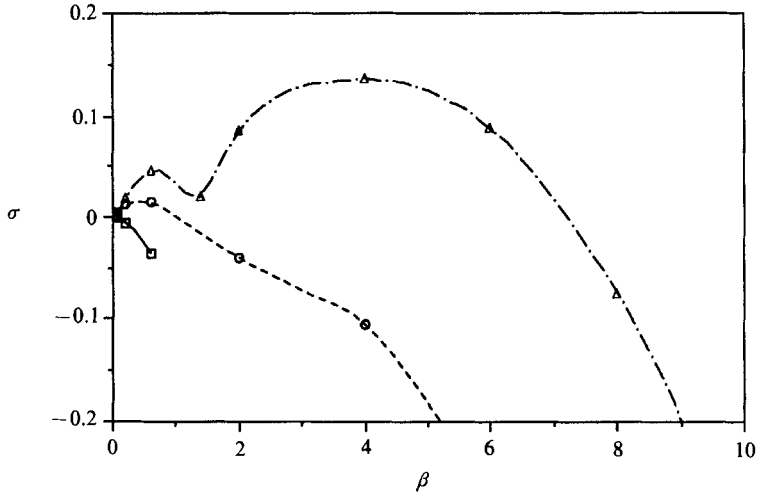

FIGURE 7. Linear growth rates, σ, of wavy disturbances are shown as a function of β for $Ro = 0.1$, $\alpha = 6$, and Re as follows: □, ——, $Re = 1.173Re_c$; ○, — — — —, $Re = 2.053Re_c$; △, —·—, $Re = 4.032Re_c$.

modes can be unstable at $\alpha = 8$. Reducing the rotation rate to $Ro = 0.1$ with $\alpha = 6$, again both modes can be unstable. Figure 7 gives $\sigma(\beta)$ for several Re at $\alpha = 5$, $Ro = 0.1$. Marginal stability to wavy disturbances is determined by $\beta \to 0$, but modes with $\beta > 0$ are more unstable for $Re > Re''_{ns}$. By interpolation, undulating vortices may occur for $Re > Re''_{ns} \approx 1.3Re_c$, and WVF1 for $Re > Re'_{ns} \approx 2.8Re_c$. The value of maximum growth rate for undulating vortices, $\sigma(\beta_2)$, does not reach a maximum in

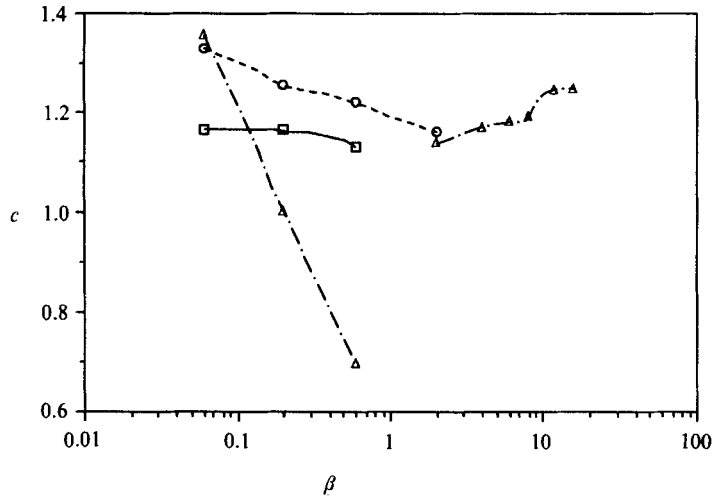

FIGURE 8. Wave speeds, c, of small-amplitude wavy disturbances to two-dimensional vortices are shown as a function of streamwise wavenumber, β, at $Ro = 0.1$, $\alpha = 6$ and Re as follows: □, ——, $Re = 1.173Re_c$; ○, — — — —, $Re = 2.053Re_c$; △, —·—, $Re = 4.032Re_c$. Data for WVF1 at $Re = 4.032Re_c$ is shown by the data to the right, and is not joined by lines to the data for WVF2 at the left.

the Re-range explored, in contrast to the behaviour for $Ro = 0.5$, $\alpha = 8$ and for undulating modes in curved channel flow (Finlay *et al.* 1988). At $Ro = 0.1$, $\beta_1 \approx 4$ is larger than β_1 at $Ro = 0.5$ or $Ro = 1.5$. Figure 7(*b*) of Alfredsson & Persson (1989) shows flow visualization at $Ro = 0.084$, $Re = 4.022Re_c$, $\alpha \approx 6$ that indicates wavy vortices having $\beta \approx 4$. Since $\beta \approx \beta_1 \gg \beta_2$, this is probably WVF1.

Figure 8 gives $c(\beta)$, corresponding to $\sigma(\beta)$ in figure 7. The comments regarding c for $Ro = 0.5$ are applicable here, except that the variation of c with α was not examined at this Ro, and $c(Re)$ varies considerably more for undulating vortices at $Ro = 0.1$ (possibly because of the larger range of Re). Wave speeds for $Ro = 0.1$ are mostly near those for $Ro = 0.5$, but are considerably lower than at $Ro = 1.5$. When non-dimensionalized by d^2/ν, instead of $d/\bar{U}, \omega$ for undulating vortices varies little with Ro; the same is not true for WVF1. (A similar non-dimensionalization yields a frequency nearly independent of Prandtl number, P, for oscillatory Rayleigh–Bénard convection rolls with stress free boundaries, but strongly dependent on P for rigid boundaries. There ν is replaced by the thermal diffusivity, Busse 1985). Wave speeds in curved channel and Taylor–Couette flow depend strongly on η (Finlay *et al.* 1988; King *et al.* 1984). Similarly, c depends on Ro.

Alfredsson & Persson (1989) almost certainly observed wavy vortices, with the waves travelling at 'about half of the undisturbed centreline velocity' ($c = 0.75$). They do not specify the parameters for this observation, although $0.015 \leqslant Ro \leqslant 0.26$. This c is lower than most values in figures 6 and 8. However, we find considerable variation of c with the various parameters, so this observation may be for Ro, α, Re, β not considered here.

Values of Re'_{ns}/Re_c and Re''_{ns}/Re_c are listed in table 2. Re''_{ns}/Re_c is nearly constant between $Ro = 0.1$ and $Ro = 0.5$ for $\alpha = 6$, and similarly between $Ro = 0.5$ and $Ro = 1.5$ for $\alpha = 8$.

The value of β observed experimentally depends on upstream conditions, nonlinear

Ro	α	Re'_{ns}/Re_c	Re''_{ns}/Re_c
0.1	6	1.3	2.8
0.5	6	Non-existent	3.0
0.5	8	1.5	2.0
1.5	8	Non-existent	2.0
1.5	10	Non-existent	2.7

TABLE 2. Values of the neutrally stable Reynolds number for onset of WVF1 (Re'_{ns}) and WVF2 (Re''_{ns}) are given at various Ro and α

mechanisms and linear growth rates. If the latter are dominant then, for $Ro = 1.5$ and $\alpha = 8, 10$, or $Ro = 0.5$ and $\alpha = 6$, only the shorter wavelength WVF1 occurs, since undulating vortices do not have positive linear growth rates. At $Ro = 0.5$, $\alpha = 8$ or $Ro = 0.1$, $\alpha = 6$, long wavelength undulating vortex flow can occur, but at higher Re, WVF1 has much higher linear growth rate. The small linear growth rates associated with undulating vortices probably make them difficult to observe experimentally because of long development lengths, as predicted for undulating vortices in curved channel flow (Finlay *et al.* 1988). As already mentioned, Alfredsson & Persson (1989) probably observed WVF1. At fixed $Re = 4.022Re_c$, and sufficiently low Ro this is the only type of waviness they observe. With increasing Ro, they observe long-wavelength wavy fluctuations. These are probably not undulating vortices, since this section indicates that these should become more difficult to observe at higher Ro.

4. Simulation of nonlinear wavy vortices

In this section we examine fully developed, three-dimensional solutions of the Navier–Stokes equations for $Re > Re'_{ns}$ or $Re > Re''_{ns}$. Channels with short streamwise lengths may not reach these states. Unless otherwise specified, all flows presented in this section have β near either β_1 or β_2 (i.e. near the most unstable β of §3), and α near that observed by Alfredsson & Persson (1989). Most of the wavy vortices in this section were obtained using the initial conditions mentioned in §3, but with the initial perturbation to the first streamwise mode having larger amplitude ($< 1\,\%\,\bar{U}$). Several runs were repeated using instead low-amplitude ($< 0.001\,\%\,\bar{U}$) random noise as initial conditions. Both initial conditions always yielded the same wavy vortex solution.

4.1. *General features*

Fully developed wavy vortices are travelling waves in which the flow pattern travels with uniform velocity c. This is similar to the behaviour of wavy Taylor vortex flow, wavy Dean vortex flow, and oscillatory Rayleigh–Bénard convection rolls. Specifically, the velocity satisfies the spatio-temporal property of a travelling wave (Rand 1982):

$$\boldsymbol{v}((x + c\Delta t) \bmod 2\pi/\beta, y, z, t + \Delta t) = \boldsymbol{v}(x, y, z, t). \tag{4.1}$$

Setting $\Delta t = 0$ in (4.1) implies streamwise periodicity with wavenumber β; setting $\Delta t = 2\pi/(c\beta)$ shows that the travelling wave has temporal periodicity with frequency $\omega = c\beta$. Values of ω for several nonlinear wavy rotating channel vortices are given in

Ro	Re/Re_c	α	β	Mode	ω	Δp	Δp (2D flow)
0.084	4.022	6	4.0	WVF1 (twisting)	4.35	0.46462	
0.084	4.022	8	4.0	WVF1 (twisting)	4.3	0.59598	0.44976
0.1	2.053	6	0.8	WVF2 (undulating)	1.00	0.23185	0.24185
0.5	1.693	8	0.2	WVF2 (undulating)	0.26	0.15998	0.22386
0.5	2.596	8	1.5	WVF1	1.30	0.24598	0.2732
0.5	3.160	6	1.5	WVF1	1.38	0.23126	0.20668
0.5	3.612	6	1.5	WVF1	1.31	0.2809	
1.5	3.277	10	1.5	WVF1	0.9	0.11306	0.091043
1.5	2.348	8	1.5	WVF1	1.0	0.069217	

TABLE 3. Frequencies, ω (obtained using temporal spectra), and values of Δp from simulation are given for nonlinear wavy vortices. Values of Δp are also given for two-dimensional vortices ($\beta = 0$) at each Ro, Re, α, except when the two-dimensional vortices are unstable to vortex doubling

table 3. These values are all within 7% of those obtained for small-amplitude waves in §3.

We simulate temporal power spectra obtained by a probe that moves at constant velocity, c_p, in the streamwise direction. In agreement with (4.1), such 'flying hot wire' spectra have ω shifted by βc_p; the results show that all frequencies with non-zero energy are integer multiples of the shifted fundamental frequency. This demonstrates that wavy rotating channel vortices are travelling waves. Fully developed two-dimensional vortices in rotating channel flow can bifurcate to two different travelling wave regimes with increasing Re.

Wavy vortices may have shift-and-reflect symmetry (Marcus 1984):

$$\left.\begin{aligned} v_y(x,y,z,t) &= v_y(x+\pi/\beta, y, -z, t), \\ v_x(x,y,z,t) &= v_x(x+\pi/\beta, y, -z, t), \\ v_z(x,y,z,t) &= -v_z(x+\pi/\beta, y, -z, t), \end{aligned}\right\} \tag{4.2}$$

where $z = 0$ is the time-averaged location of an upflow or downflow boundary. Although this symmetry was not enforced, all wavy vortices in rotating channel flow satisfy (4.2). Preliminary runs at higher Re than presented here indicate that asymmetric flows can occur in the transitions leading to chaos.

Spatial energy spectra for wavy rotating channel vortices decay exponentially with increasing Fourier wavenumber k_z or k_x (cf. Finlay 1989 for more on this for two-dimensional vortices). This behaviour occurs for wavy Taylor vortices (Marcus 1984), wavy Dean vortices (Finlay *et al.* 1988) and oscillatory Rayleigh–Bénard convection rolls (Curry *et al.* 1984). The adequacy of our spatial resolution is monitored by observing whether such exponential behaviour occurs up to the maximum wavenumber resolved ($19 \times 33 \times 19$ modes in x, y, z are used for all runs in this section).

Between vortices the flow is directed mostly toward positive or negative y, i.e. these are upflow or downflow regions. The upflow region has higher $|v_y|$ than the downflow region. For rotating Poiseuille flow, the lower wall at $y = -\frac{1}{2}$ has higher pressure and the flow near it ($y < 0$) is inviscidly unstable; the opposite is true of the upper wall. Larger $|v_y|$ thus occurs in the upflow regions where flow is away from the higher pressure, inviscidly unstable wall. Similarly, for curved channel vortices, radial velocities are highest in the regions with radially inward flow (inflow)

away from the higher pressure, inviscidly unstable outer wall (Finlay *et al.* 1988). In contrast, Taylor vortices have strongest radial flow towards the higher pressure outer wall (Marcus 1984).

A measure of the strength of the vortices is the pressure gradient parameter Δp, defined as

$$\Delta p \equiv \left(\overline{\frac{\partial p}{\partial x}} - \frac{\partial P}{\partial x}\right) \Big/ \frac{\partial P}{\partial x}, \tag{4.3}$$

where $\partial p/\partial x$ is the streamwise pressure gradient, $\overline{\partial p}/\partial x$ is the value of $\partial p/\partial x$ averaged over the computational box, and $\partial P/\partial x$ is the streamwise pressure gradient for Poiseuille flow. The quantity Δp plays a role similar to that of the Nusselt number in Rayleigh–Bénard convection, and the non-dimensional torque in Taylor–Couette flow. Values of Δp for several nonlinear wavy vortex flows and corresponding two-dimensional vortices are given in table 3. For the two cases of undulating vortices Δp is lower than for (unstable) two-dimensional vortices at the same Re, α, Ro. This is similar to wavy Taylor vortices and undulating Dean vortices, which have lower torque and Δp, respectively, than the corresponding axisymmetric vortex flow. In contrast, all but one of the WVF1 ($\alpha = 8$, $Re = 2.596 Re_c$, $\beta = 1.5$, $Ro = 0.5$) have higher Δp than the corresponding unstable two-dimensional vortex flow. Twisting Dean vortices also cause Δp to be higher.

By their absence or presence, the following few qualitative features capture the essential temporal and streamwise variation of wavy vortex flows (because the flows are due to fully developed travelling waves, temporal and streamwise variation are equivalent). If significant variations in vortex strength occur, one vortex is strongest when the other is weakest. The vortices may oscillate back and forth in the spanwise direction; this will be referred to as sideslipping. Independent of this motion, vortex rocking will be said to occur if the line (in a (y, z)-plane) joining two vortex centres across an upflow region oscillates from positive to negative slope. Finally, the upflow and downflow regions may have significant and varying v_z, causing directional changes of the upflow and downflow regions.

Rocking, sideslipping and directional changes in the upflow region are observed to occur together in the following patterns. For all wavy vortices, large sideslipping motion occurs only in the direction opposite to the spanwise velocities in the upflow region. Wavy vortices having large maximum sideslip ($> 0.3\lambda$), and directional changes of the upflow region that are approximately in phase with rocking (i.e. in a (y, z)-plane, the upflow region is approximately perpendicular to the line joining two vortex centres), with no other outstanding features, will be called undulating vortices. All WVF2 are undulating vortices. No WVF1 is an undulating vortex flow. For these reasons, WVF2 and undulating vortex flow will be used synonymously. Wavy vortices that sideslip only a little ($< 0.1\lambda$), but have the latter property of undulating vortices, and no other outstanding features, will be called twisting vortices. All wavy vortices observed by Finlay *et al.* (1988) in curved channel flow were undulating or twisting (for curved channel flow, 'upflow' is replaced by 'inflow'). For WVF1, vortex rocking is characterized by two features: (1) if one vortex in a pair is considerably stronger than the other, then the weak vortex moves rapidly to the $y = -\frac{1}{2}$ wall soon after it is weakest; (2) significant motion of a vortex centre toward the $y = +\frac{1}{2}$ wall occurs at locations other than where the vortex is weakest.

With these features in mind, we now examine some wavy vortex velocity fields.

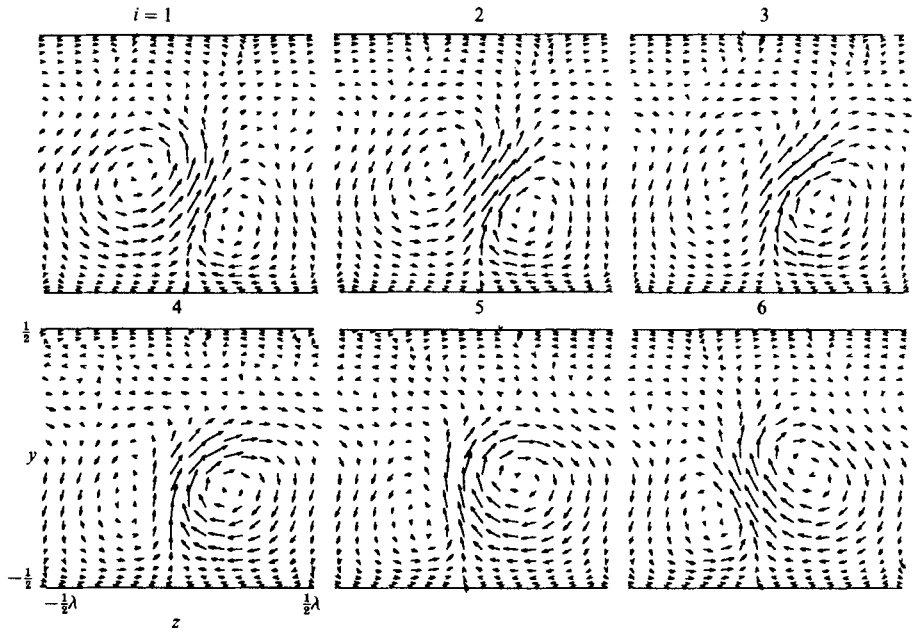

FIGURE 9. WVF1 (twisting vortices) at $Ro = 0.084$, $Re = 4.022Re_c$, $\alpha = 6$, $\beta = 4$ is projected onto (y,z)-planes for $x = (2\pi/\beta)(i/10)$, $i = 0, 1, 2, \ldots, 5$. All six plots have axes as given in the $i = 4$ plot. Plots for $6 \leqslant i \leqslant 10$ are a reflection about $z = 0$ of the plot at $i-5$.

4.2. *Wavy vortices for small Ro*

Shown in figure 9 are arrow plots of the cross-flow velocities for fully developed WVF1 with $Ro = 0.084$, $Re = 4.022Re_c$, $\alpha = 6$, $\beta = 4$. These are approximately the same Ro, Re, α, β as figure 7 (*b*) of Alfredsson & Persson (1989). The plots represent the cross-flow velocities for a sequence of (y,z)-planes. The streamwise flow is perpendicular to and into the plane of the plots. Only half a streamwise wavelength is shown, since the other half of the sequence is obtained from the shift-and-reflect property (4.2). All vector plots herein are drawn with the average spanwise location of the upflow region as midplane. For visual clarity, not all grid-point velocities are shown. Since the flow is a travelling wave, figure 9 is equivalent to a temporal sequence of the cross-flow velocities at one streamwise location. This flow has the features of twisting vortices and bears remarkable resemblance to twisting Dean vortices shown in figure 16 of Finlay *et al.* (1988). (The outer curved channel wall corresponds to the $y = -\frac{1}{2}$ wall here, so each plot must be turned upside down to match figure 16 there.) Using $\alpha = 8$ at the same Re, Ro, β yields a flow that is qualitatively unchanged from figure 9. The flow observed by Alfredsson & Persson (1989) at this Re, Ro is probably a WVF1 having the qualitative features of twisting vortices mentioned in §4.1.

Arrow plots of the cross-flow velocities for undulating vortices with $Ro = 0.1$, $Re = 2.053Re_c$, $\alpha = 6$, $\beta = 0.8$ are shown in figure 10. For the same reasons as figure 9, only half a streamwise wavelength is shown. This flow is very similar to undulating Dean vortices (figure 15 of Finlay *et al.* 1988), and wavy Taylor vortices (figure 6 of Marcus 1984); all share the qualitative features mentioned previously for undulating vortices.

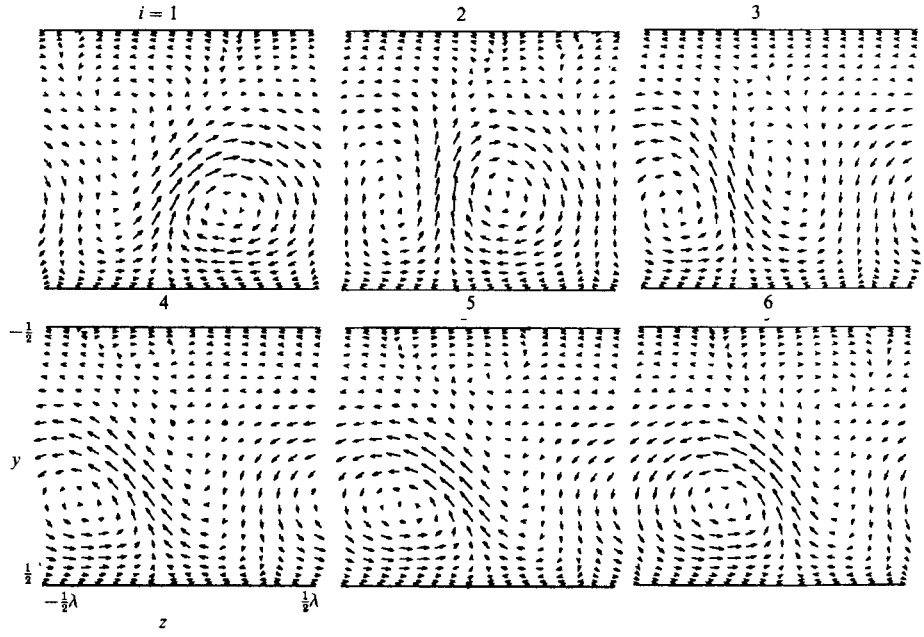

FIGURE 10. WVF2 (undulating vortices) at $Ro = 0.1$, $Re = 2.053Re_c$, $\alpha = 6$, $\beta = 0.8$ is projected onto (y, z)-planes. See the caption of figure 9 for more explanation.

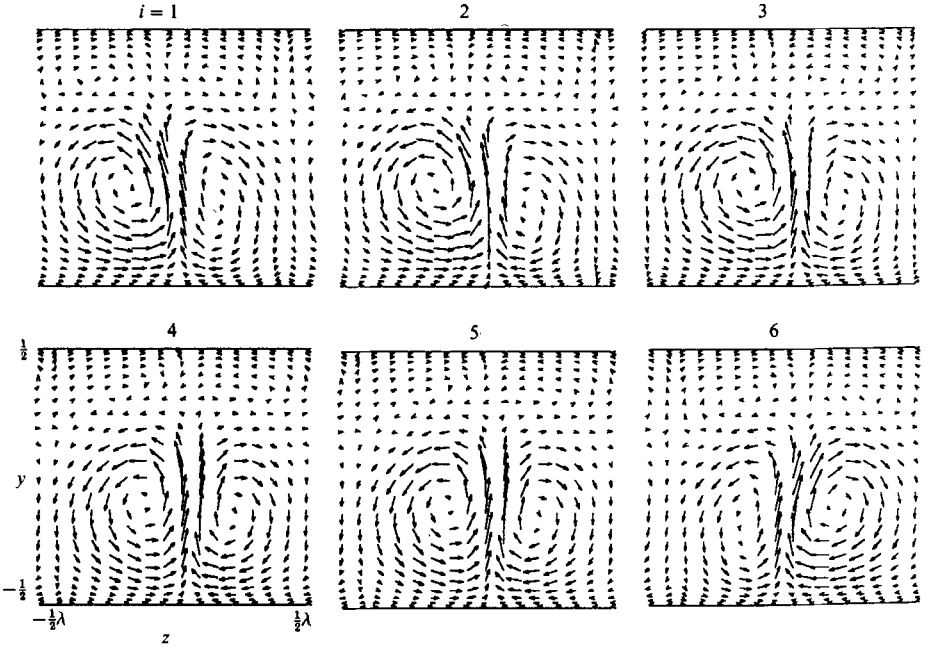

FIGURE 11. WVF1 at $Ro = 0.5$, $Re = 3.160Re_c$, $\alpha = 6$, $\beta = 1.5$ is projected onto (y, z)-planes. See the caption of figure 9 for more explanation.

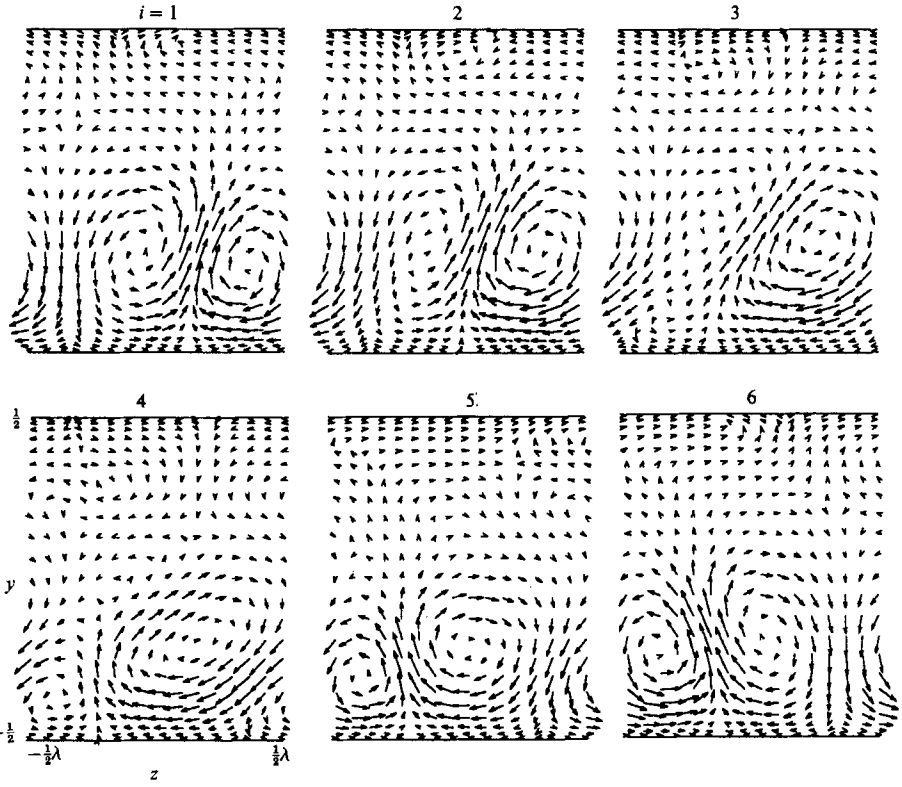

FIGURE 12. WVF1 at $Ro = 0.5$, $Re = 2.596Re_c$, $\alpha = 8$, $\beta = 1.5$ is projected onto (y,z)-planes. See the caption of figure 9 for more explanation.

4.3. *Wavy vortices at* $Ro = 0.5$

At $Ro = 0.5$ and $\alpha = 6$, §3 indicates that undulating vortices are not possible. WVF1 with $Re = 3.160Re_c$, $\beta = 1.5$ at this α, Ro is shown in figure 11. (Arrows of the same length in figures 9, 10 and 11 have non-dimensional velocity magnitudes of the same value.) The directional changes of velocity in the upflow region are considerably smaller than for any other wavy vortices examined so far. The vortices rock with little sideslipping, like twisting vortex flow, but the directional changes in the upflow jet lag considerably behind the rocking, so the term 'twisting vortices' cannot be applied as defined previously.

WVF1 with $\alpha = 8$, $Re = 2.596Re_c$, and the same Ro, β as figure 11, is shown in figure 12. This α is higher than observed at this Ro by Alfredsson & Persson (1989). Figure 12 shows the only WVF1 found with large sideslipping. Large sideslipping in conjunction with directional changes of the upflow region that are in phase with vortex rocking would make this flow like undulating vortices; however, one of the vortices disappears once per period, which is unlike undulating vortex flow, or any other wavy vortex flow. This flow is also the only WVF1 which has lower Δp than the corresponding two-dimensional vortex flow.

At $Ro = 0.5$, undulating vortices are possible at $\alpha = 8$, although this α is greater than any α observed by Alfredsson & Persson (1989). For $\alpha = 8$, $Ro = 0.5$, and $Re = 1.693Re_c$, $\beta = 0.2$, vortex rocking is less pronounced than other undulating vortices, but the flow is similar to that in figure 10.

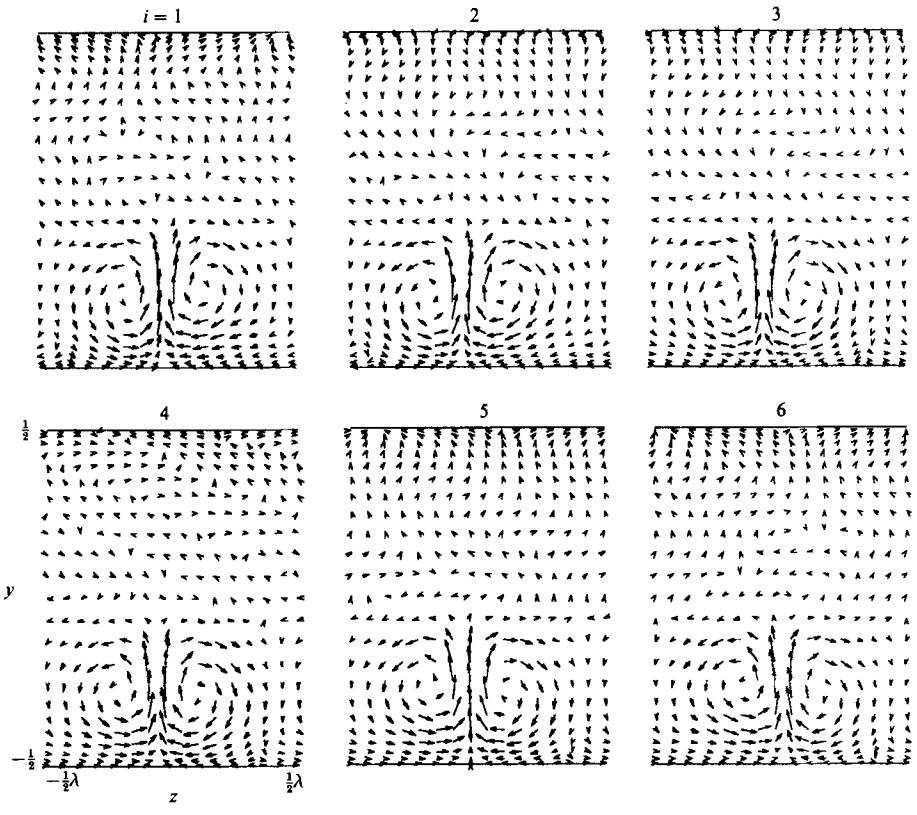

FIGURE 13. WVF1 at $Ro = 1.5$, $Re = 2.348Re_c$, $\alpha = 8$, $\beta = 1.5$ is projected onto (y, z)-planes. See the caption of figure 9 for more explanation.

4.4. *Wavy vortices at* $Ro = 1.5$

At $Ro = 1.5$, §3 indicates only WVF1 is possible. Experimental data on vortex spacing is unavailable at such a high rotation rate, so we choose α near $\alpha_c = 8.13$. WVF1 with $\alpha = 8$, $Re = 2.348Re_c$, $\beta = 1.5$, is shown in figure 13. There is little vortex rocking, sideslipping, or variation in vortex strength. Unlike either the twisting or undulating patterns, the changes of the v_z velocities in the upflow region are 180° out of phase with rocking and are very small.

Wavy vortices at the same Ro, β, but $\alpha = 10$, $Re = 3.277Re_c$ are shown in figure 14. The flow is different again. Considerable vortex rocking occurs, with more sideslip (maximum sideslip is $\approx 0.4\lambda$) than twisting vortices. Unlike either twisting or undulating patterns, significant phase difference exists between vortex rocking and changes in upflow direction.

At $Ro = 1.5$ the vortices are located closer to the $y = -\frac{1}{2}$ wall than at lower Ro. Significant v_y, v_z velocities exist only for $y < 0$. For $y > 0$ the secondary flow is weak, but quite complicated.

Wavy vortex flows examined at $Ro = 1.5$ resemble neither undulating nor twisting vortices.

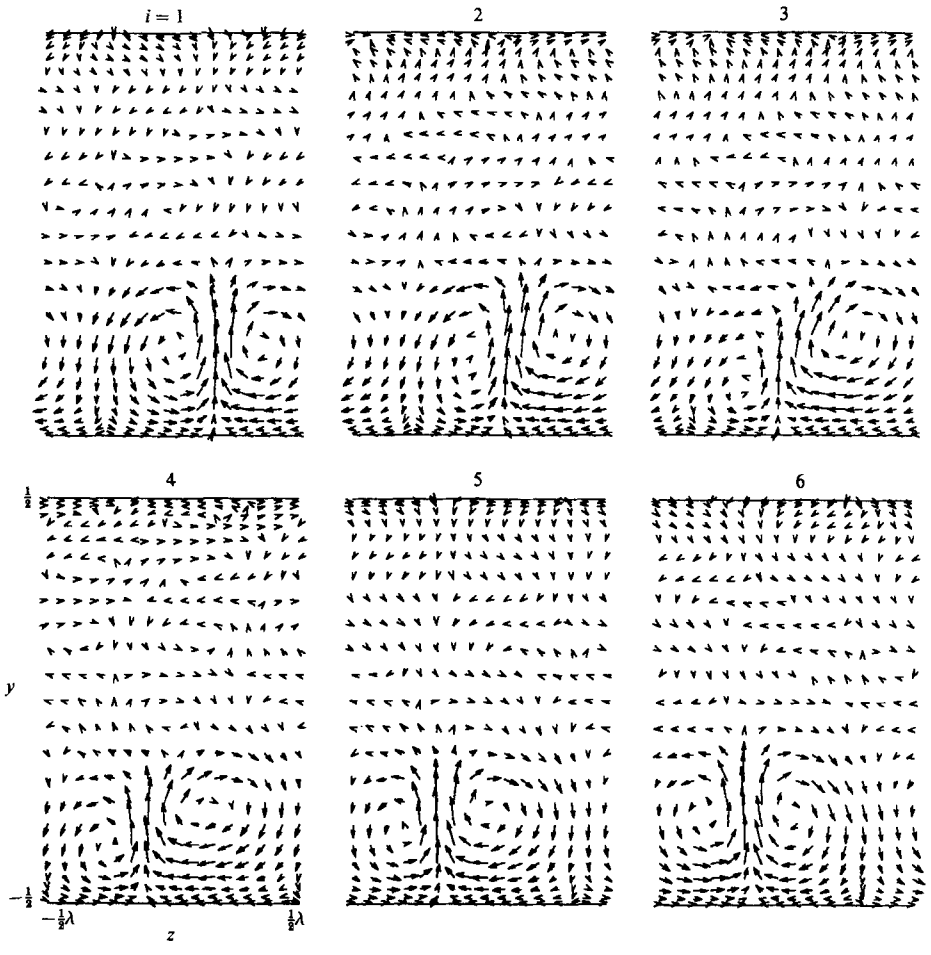

FIGURE 14. WVF1 at $Ro = 1.5$, $Re = 3.277Re_c$, $\alpha = 10$, $\beta = 1.5$ is projected onto (y, z)-planes. See the caption of figure 9 for more explanation.

5. Summary

Three-dimensional simulations were used to study wavy vortices in rotating channel flow. Linear stability of two-dimensional vortices to wavy disturbances shows that two wavy modes are possible: WVF1 and WVF2. WVF1 occurs for all Ro examined and for $Re > Re'_{ns}$, where $2 \leqslant Re'_{ns}/Re_c \leqslant 3$ for $0.1 \leqslant Ro \leqslant 1.5$ (Re_c is the critical Re for instability of rotating plane Poiseuille flow to two-dimensional vortices). Regular oscillations observed experimentally by Alfredsson & Persson (1989) were likely due to WVF1. WVF2 is possible only at lower rotation rates and $Re > Re''_{ns}$, where $Re''_{ns}/Re_c \approx 1.3$–$1.5$. At Ro where both modes occur, WVF2 occurs first with increasing Re, i.e. $Re''_{ns} < Re'_{ns}$, but at sufficiently high Re, WVF1 has much higher linear growth rate. Small-amplitude wavy disturbances have wave speeds that are generally not weakly dependent on Re, α, β or Ro. Nonlinear wavy vortices are travelling waves with wave speeds near those obtained from linear stability analysis. WVF1 and WVF2 satisfy shift-and-reflect symmetry about their mean upflow and downflow planes. Wavy vortices vary considerably in appearance with

Ro and α, but can be characterized qualitatively by the following features: rocking, sideslipping, and regular changes in the direction of upflow regions between vortices. In these features, WVF1 varies greatly with *Ro* and α, but is like twisting Dean vortex flow (Finlay *et al.* 1988) for low *Ro*. In contrast, WVF2 varies far less in qualitative appearance and has the features of undulating Dean vortices (Finlay *et al.* 1988), and wavy Taylor vortices (Marcus 1984). Based on linear growth rates, WVF1 should dominate experimentally.

The author gratefully acknowledges the CPU time supplied by Cray Canada Inc. and the financial support of NSERC.

REFERENCES

ALFREDSSON, P. A. & PERSSON, H. 1989 Instabilities in channel flow with system rotation. *J. Fluid Mech.* **202**, 543–557.

BOLTON, E. W., BUSSE, F. H. & CLEVER, R. M. 1986 Oscillatory instabilities of convection rolls at intermediate Prandtl numbers. *J. Fluid Mech.* **164**, 469–485.

BUSSE, F. H. 1972 The oscillatory instability of convection rolls in a low Prandtl number fluid. *J. Fluid Mech.* **52**, 97–112.

BUSSE, F. H. 1985 Transition to turbulence in Rayleigh–Bénard convection. In *Hydrodynamic Instabilities and the Transition to Turbulence*, 2nd edn (ed. H. L. Swinney & J. P. Gollub), Topics in Applied Physics, vol. 45, pp. 97–137. Springer.

CANUTO, C., HUSSAINI, M. Y., QUARTERONI, A. & ZANG, T. A. 1988 *Spectral Methods in Fluid Dynamics*. Springer.

CLEVER, R. M. & BUSSE, F. H. 1974 Transition to time-dependent convection. *J. Fluid Mech.* **65**, 625–645.

CURRY, J. H., HERRING, J. R., LONCARIC, J. & ORSZAG, S. A. 1984 Order and disorder in two- and three-dimensional Bénard convection. *J. Fluid Mech.* **147**, 1–38.

DAVEY, A., DIPRIMA, R. C. & STUART, J. T. 1968 On the instability of Taylor vortices. *J. Fluid Mech.* **31**, 17–52.

DIPRIMA, R. C. & SWINNEY, H. L. 1985 Instabilities and transition in flow between concentric rotating cylinders. In *Hydrodynamic Instabilities and the Transition to Turbulence*, 2nd edn (ed. H. L. Swinney & J. P. Gollub), Topics in Applied Physics, vol. 45, pp. 139–180. Springer.

FINLAY, W. H. 1989 Perturbation expansion and weakly nonlinear analysis for two-dimensional vortices in curved or rotating channels. *Phys. Fluids* A **1**, 854–860.

FINLAY, W. H., KELLER, J. B. & FERZIGER, J. H. 1987 Instability and transition in curved channel flow. *Rep.* TF-30, Dept. of Mech. Engng, Stanford University, CA.

FINLAY, W. H., KELLER, J. B. & FERZIGER, J. H. 1988 Instability and transition in curved channel flow. *J. Fluid Mech.* **194**, 417–456.

HART, J. E. 1971 Instability and secondary motion in a rotating channel flow. *J. Fluid Mech.* **45**, 341–351.

JONES, C. A. 1981 Nonlinear Taylor vortices and their stability. *J. Fluid Mech.* **102**, 249–261.

JONES, C. A. 1985 The transition to wavy Taylor vortices. *J. Fluid Mech.* **157**, 135–162.

KHESGHI, H. S. & SCRIVEN, L. E. 1985 Viscous flow through a rotating square channel. *Phys. Fluids* **28**, 2968–2979.

KING, G. P., LI, Y., LEE, W., SWINNEY, H. L. & MARCUS, P. S. 1984 Wave speeds in wavy Taylor vortex flow. *J. Fluid Mech.* **141**, 365–390.

KUZ'MINSKII, L. V., SMIRNOV, E. M. & YURKIN, S. V. 1983 Longitudinal cellular structures of Taylor–Görtler type vortices on the high-pressure side of rotating channels. *J. Appl. Mech. Tech. Phys.* **24**, 882–886.

LEZIUS, D. K. & JOHNSTON, J. P. 1976 Roll-cell instabilities in rotating laminar and turbulent channel flows. *J. Fluid Mech.* **77**, 153–175.

LIGRANI, P. & NIVER, R. D. 1988 Flow visualization of Dean vortices in a curved channel with 40 to 1 aspect ratio. *Phys. Fluids* **31**, 3605–3618.

MARCUS, P. S. 1984 Simulation of Taylor–Couette flow. Part 2. Numerical results for wavy-vortex flow with one travelling wave. *J. Fluid Mech.* **146**, 65–113.

MEYER-SPASCHE, R. & KELLER, H. B. 1985 Some bifurcation diagrams for Taylor vortex flows. *Phys. Fluids* **28**, 1248–1252.

MOSER, R. D. & MOIN, P. 1984 Direct numerical simulation of curved turbulent channel flow. *NASA TM* 85974.

MOSER, R. D. & MOIN, P. 1987 The effects of curvature in wall-bounded turbulent flow. *J. Fluid Mech.* **175**, 497–510.

MOSER, R. D., MOIN, P. & LEONARD, A. 1983 A spectral numerical method for the Navier–Stokes equations with applications to Taylor–Couette flow. *J. Comput. Phys.* **52**, 524–544.

NG, L., SINGER, B. A., HENNINGSON, D. S. & ALFREDSSON, P. H. 1989 Instabilities in rotating channel flow. In *Instability and Transition* (eds. M. Hussaini & R. Voigt). Springer.

RAND, D. 1982 Dynamics and symmetry. Predictions for modulated waves in rotating fluids. *Arch. Rat. Mech. Anal.* **79**, 1–37.

SMIRNOV, E. M. & YURKIN, S. V. 1983 Fluid flow in a rotating channel of square section. *Fluid Dyn.* **18**, 850–855.

SPEZIALE, C. G. 1982 Numerical study of viscous flow in rotating rectangular ducts. *J. Fluid Mech.* **122**, 251–271.

SPEZIALE, C. G. & THANGAM, S. 1983 Numerical study of secondary flows and roll-cell instabilities in rotating channel flow. *J. Fluid Mech.* **130**, 377–395.

THANGAM, S. & SPEZIALE, C. G. 1985 Numerical study of thermal convection in rotating channel flow. *Intl J. Num. Meth. Fluids* **5**, 133–154.

THANGAM, S. & SPEZIALE, C. G. 1987 Non-Newtonian secondary flows in ducts of rectangular cross-section. *Acta Mech.* **68**, 121–138.

TRITTON, D. J. & DAVIES, P. A. 1985 Instabilities in geophysical fluid dynamics. In *Hydrodynamic Instabilities and the Transition to Turbulence*, 2nd edn (ed. H. L. Swinney & J. P. Gollub), Topics in Applied Physics, vol. 45, pp. 229–270. Springer.

YANG, K. & KIM, J. 1990 Numerical investigation of instability and transition in rotating plane Poiseuille flow. Submitted to *Phys. Fluids* A.